PHYSICAL REVIEW B **105**, 235141 (2022)

Editors' Suggestion

Fluctuating spin-orbital texture of Rashba-split surface states in real and reciprocal space

Takuto Nakamura,[1,2,*] Yoshiyuki Ohtsubo,[3,1,2,†] Ayumi Harasawa,[4] Koichiro Yaji,[5] Shik Shin,[4]
Fumio Komori,[4,‡] and Shin-ichi Kimura[1,2,6,§]
[1]*Graduate School of Frontier Biosciences, Osaka University, Suita 565-0871, Japan*
[2]*Department of Physics, Graduate School of Science, Osaka University, Toyonaka 560-0043, Japan*
[3]*National Institutes for Quantum Science and Technology, Sendai 980-8579, Japan*
[4]*Institute for Solid State Physics, The University of Tokyo, Kashiwa 277-8581, Japan*
[5]*National Institute for Materials Science, Tsukuba, Ibaraki 305-0003, Japan*
[6]*Institute for Molecular Science, Okazaki 444-8585, Japan*

(Received 28 March 2022; accepted 7 June 2022; published 27 June 2022)

Spin-orbit interaction in low-dimensional systems, namely, Rashba systems and the edge states of topological materials, has been extensively studied in this decade as a promising source to realize various fascinating spintronic phenomena, such as the source of the spin current and spin-mediated energy conversion. Here, we show the odd fluctuation in the spin-orbital texture in a surface Rashba system on Bi/InAs(110)-(2 × 1) by spin- and angle-resolved photoelectron spectroscopy and a numerical simulation based on a density-functional theory (DFT) calculation. The surface state shows a paired parabolic dispersion with the spin degeneracy lifted by the Rashba effect. Although its spin polarization should be fixed in a particular direction based on the Rashba model, the observed spin polarization varies greatly and even reverses its sign depending on the wave number. DFT calculations also reveal that the spin directions of two inequivalent Bi chains on the surface change from nearly parallel (canted parallel) to antiparallel in real space in the corresponding wave vector region. These results point out an oversimplification of the nature of spin in Rashba and Dirac systems and provide more freedom than expected for spin manipulation of photoelectrons.

DOI: 10.1103/PhysRevB.105.235141

I. INTRODUCTION

The symmetry breaking of a system often causes fertile unconventional physical phenomena, such as nematic superconductivity appearing with rotational asymmetry [1] and orbital-angular-momentum polarization of graphene Dirac-cone states caused by the asymmetry between sublattices of a honeycomb lattice (pseudospin) [2]. In particular, spin-orbit interaction (SOI) in two-dimensional (2D) surface systems without three-dimensional (3D) translation and space-inversion symmetry in the bulk (3D) crystal, namely, the Rashba effect [3] and edge states of topological materials [4], is a promising source to host, create, or convert spin-polarized electrons without magnetic materials and fields [5,6].

A schematic of SOI-caused helical spin polarization in a 2D system is depicted in Fig. 1(a), where surface electrons are polarized toward the orientation perpendicular to both the wave vector and the surface normal. In this model, the potential gradient at the surface is assumed to be parallel to the surface normal. An electron moving in such a potential gradient experiences an effective magnetic field $\vec{B}_{\mathrm{eff}} \propto \vec{E} \times \vec{k}$ resulting in Zeeman-like splitting and spin polarizations parallel and antiparallel to $\vec{B}_{\mathrm{eff}}$ [3]. This can be regarded as the outcome of the symmetry breaking in the 2D system along the out-of-plane orientation. In this model, one spin-split branch of the surface band always holds one spin orientation, the so-called spin-momentum locking, clockwise (CW) or counterclockwise (CCW) in reciprocal space. This assumption is consistent with spin- and angle-resolved photoelectron spectroscopy (SARPES) data reported by the early 2010s except for few cases and is widely used in the interpretation of surface-spin-mediated energy conversion experiments [6].

Although such a model is based on a simple and intuitive picture, following studies revealed that the actual case is more sophisticated than the model is. The in-plane asymmetry also contributes to the surface spin polarization, although it is not included in the simple Rashba model considered above. For example, out-of-plane spin polarization in triangular surface lattices, i.e., valley polarization, is caused by the lack of in-plane twofold rotation symmetry [7–10]. Moreover, recent studies, by using the combination of SARPES and theoretical calculation, revealed the contribution of complex combinations of spin and orbital terms in the wave functions to 2D spin-polarized surface states, even in a single surface band [11–13]. These studies suggested that the Rashba model with only the CW and CCW spin orientations is oversimplified. However, no one knows the degree of the oversimplification, in other words, how freely the electron spins could orient, in the actual surface electronic systems with SOI so far. One difficulty of such research is that most of the surface systems known to host Rashba-type spin-split states have many symmetry operations, such as C_{3v} rotation and mirror planes,

---

[*] nakamura.takuto.fbs@osaka-u.ac.jp

[†] y_oh@qst.go.jp

[‡] Present address: Institute of Industrial Science, The University of Tokyo, Tokyo 153-8505, Japan.

[§] kimura.shin-ichi.fbs@osaka-u.ac.jp

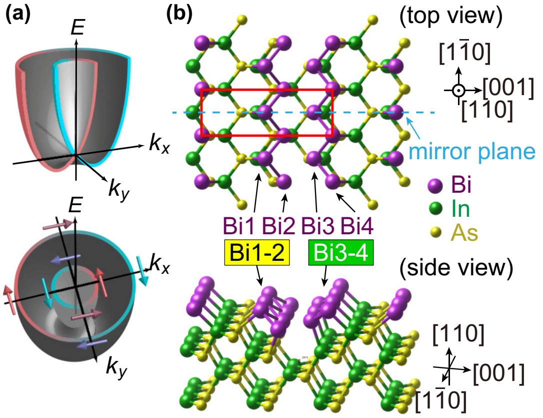

FIG. 1. Schematic of conventional Rashba-type spin-split bands and surface atomic structure of Bi/InAs(110)-(2 × 1). (a) Ideal two-dimensional spin-split electronic bands due to Rashba-type SOI. The spin polarization direction is perpendicular to the wave vector $\vec{k}$, exhibiting a helical spin polarization in reciprocal space. (b) Surface atomic structure of Bi/InAs(110)-(2 × 1). Tilted atomic chains of Bi on the InAs(110) substrate form the (2 × 1) surface superlattice, which consists of four nonequivalent Bi atoms, Bi1, Bi2, Bi3, and Bi4, as indicated. The thin solid rectangle is the (2 × 1) surface unit cell, and the dashed line is the mirror plane, which is the unique symmetry operation in this surface atomic structure.

as well as a small number of inequivalent surface atoms in the unit cell; these behave as strict constraint conditions for spin polarization. Therefore, to reveal the actual degree of freedom in surface spin polarization and distinguish it from the coexisting restrictions from surface symmetry operations which do not always exist in general surface systems, it is important to observe the spin-split surface states on the surface with (i) a small number of symmetry operations and (ii) a large number of inequivalent surface atoms.

In this work, we study the spin and orbital texture in the surface electronic states of Bi/InAs(110)-(2 × 1) using SARPES and a numerical simulation based on density-functional theory (DFT) calculations. The (2 × 1) superlattice of Bi on InAs(110) consists of two inequivalent and tilted Bi chains, as depicted in Fig. 1(b) [14]. This surface structure holds a small number of surface symmetry operations, only one mirror plane, and no rotation and thus is an ideal test case to study the minimal feature of surface SOI in lower-symmetry systems. Actually, the surface state exhibited an unconventional spin fluctuation. The sign on the surface spin polarization modulated independently in the two nonequivalent surface atomic chains and even in a single band, its sign inverted depending on the wave number. It was found that the two inequivalent Bi chains exhibit even antiferromagnetic spin configurations at the same binding energy and wave number. These results point out an oversimplification of the nature of spin in surface 2D systems and suggest more freedom than expected.

II. METHODS

The surface of InAs(110) substrates was cleaned by repeated cycles of Ar ion sputtering (1 keV) and annealing (700 K). After the cleaning, a sharp (1 × 1) electron diffraction pattern was confirmed by using low-energy electron diffraction (LEED). Next, a few monolayers of Bi were deposited on InAs(110)-(1 × 1) from a Knudsen cell at room temperature. Subsequent annealing at 600 K for 20 min resulted in a Bi/InAs(110) surface exhibiting a sharp (2 × 1) surface reconstruction pattern. The LEED diffraction patterns are shown in Fig. S1 in the Supplemental Material [15].

ARPES and SARPES measurements were performed at the Institute for Solid State Physics, The University of Tokyo, with a linearly polarized laser source ($h\nu = 6.994$ eV) [16]. The photoelectrons were detected along the $\bar{\Gamma}$-$\bar{X}$ high-symmetry line in the (2 × 1) surface Brillouin zone, as shown in Fig. 2(e). In this experimental geometry, the planes of photon incidence and photoelectron detection were common. The energy resolution and the position of E_{F} were calibrated by the Fermi edge of a Cu block attached to the samples. The energy resolution for the ARPES (SARPES) measurements was set to ∼9 meV (∼20 meV). The effective Sherman function of a very low energy electron diffraction type spin detector was set to 0.27. The sample temperature was kept at 45 K during the ARPES and SARPES experiments.

The initial states and their spin polarization of the Bi/InAs(110) surface were obtained by using a DFT calculation based on the "augmented plane wave + local orbitals" method implemented in the WIEN2K code with SOI considered [17]. We adopted the modified Becke-Johnson potential combined with a local density approximation to construct the exchange and correlation potentials [18,19]. The surface atomic structure was modeled by 20 layers of InAs with a surface covered with (2 × 1) zigzag Bi chains. The surface atomic structure was energetically optimized down to the third In and As layers, and the rest of the substrate atom positions were fixed to those in the bulk InAs single crystal. The eventual surface atomic structure model was almost identical to the model obtained experimentally [14].

The spin polarization of the photoelectrons was numerically calculated considering the interference in the final-state spinors. For this calculation, we assumed the photoexcitation process from the inequivalent initial-state wave functions, the two different Bi chains, obtained by the DFT calculation above. The final state was set as a spin-integrated free electron. The spinor interference was calculated in a manner similar to that in Refs. [11,13] (see Supplemental Material, Note 1 [15], for details).

III. RESULTS AND DISCUSSION

A. Photoelectron spectra of spin-polarized surface electronic states

Figures 2(a) and 2(b) show conventional (spin-integrated) ARPES band dispersions along $\bar{\Gamma}$-$\bar{X}$ using *s*- and *p*-polarized photons, respectively. The experimental geometry and definitions of the incident-photon polarizations of the (S)ARPES experiment are shown in Fig. 2(e). As shown in a previous work [20], surface bands (S and S') were observed below the Fermi level E_{F} with paired parabolic dispersion around the surface Brillouin zone center ($k_{y//[\bar{1}10]} = 0$ Å^{-1}). The photoelectron intensity of S with *s* polarization was

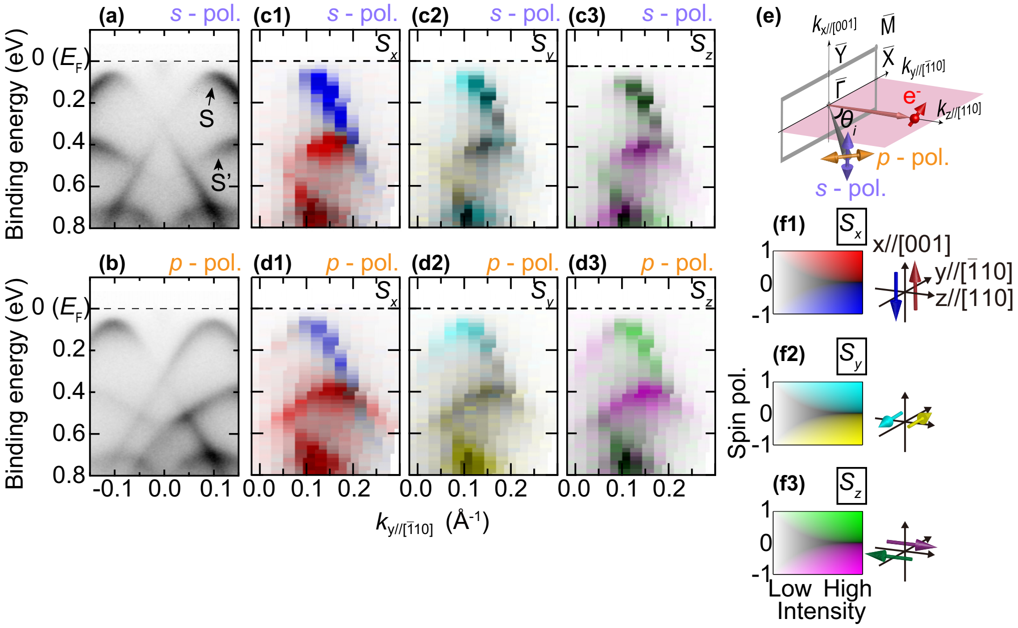

FIG. 2. Spin-polarized surface band structures measured by SARPES. (a) and (b) ARPES and (c) and (d) SARPES 2D plots measured with *s*-polarized (top) and *p*-polarized (bottom) photons along $\bar{\Gamma}$-$\bar{X}$ (parallel to the Bi chains). (a) and (b) Spin-integrated ARPES intensity maps. The photon incident angle θ_i is 50°. SARPES maps polarized to (c1) and (d1) S_x, (c2) and (d2) S_y, and (c3) and (d3) S_z. The spin orientations are defined in (f). θ_i is 38°. (e) Experimental geometry of the SARPES measurements and definitions of the coordinates. The (2 × 1) surface Brillouin zone and the common plane of the photon incidence and photoelectron detection are superposed simultaneously. (f) Definitions of the spin directions of the photoelectrons. The colors of the SARPES intensity plots are determined based on the photoelectron intensity and spin polarization, as indicated in these 2D color maps.

diminished around $k_{y//[\bar{1}10]} = 0$ Å^{-1}, suggesting the influence of the photoexcitation selection rule [21]. Assuming the nearly-free-electron final state, photoelectrons from the initial states with odd and even parities with respect to the measurement plane [see Fig. 2(e)] should be excited by *s*- and *p*-polarized photons, respectively. This suggests that the inner part of the parabolic *S* band is mainly composed of wave functions with even symmetry, whereas the outer part is from multiple wave functions with both even and odd symmetries.

Figures 2(c1)–2(c3) and 2(d1)–2(d3) show polarization-dependent SARPES maps obtained using *s*- and *p*-polarized photons, respectively. These are two-dimensional color plots of photoelectron intensity and magnitude of spin polarization [see Figs. 2(f1)–2(f3) for their definitions]. The corresponding spin-resolved energy distribution curves are also shown in Fig. S2 in the Supplemental Material [15]. The band dispersion obtained by SARPES intensities shown in Figs. 2(c1)–2(d3) agrees well with the spin-integrated ones in Figs. 2(a) and 2(b). Figures 2(c1) and 2(d1) show spin polarization along the S_x direction. This orientation is in plane and perpendicular to the wave vector, which is expected from the simple 2D model depicted in Fig. 1(a). However, in contrast to the simple model, Fig. 2(d1) shows that the S_x spin polarization direction varies in a single parabolic band (*S*) with the same sign of $k_{y//[\bar{1}10]}$. Such a peculiar spin modulation is not observed in Fig. 2(c1), indicating the effect of incident photon polarizations (*s* and *p*). Thus far, it has been reported in some topological materials that switching the photon polarization could change the spin polarization of photoelectrons [11,13].

In contrast to *S*, another spin-polarized band, *S*′, shows unidirectional polarization in the entire $k_{y//[\bar{1}10]}$ range. Therefore, we focus on the spin polarization of *S* in the following in order to investigate this peculiar behavior.

In addition to S_x, spin polarizations of the other spin directions, S_y and S_z, are observed in Figs. 2(c2)–2(c3) and 2(d2)–2(d3). S_z is almost zero with *s*-polarized photons but has a finite value with *p*-polarized photons. Although the S_z polarization normal to the surface is not expected from the simplest model, as shown in Fig. 1(a), this polarization is allowed with an in-plane potential gradient, as reported in some 2D systems without twofold rotation [7,8,10]. However, the spin reversal of S_x in the single band [Fig. 2(d3)] is peculiar. Moreover, in this measurement, an evident spin polarization parallel to the wave vector (S_y) is also observed with both photon polarizations, as shown in Figs. 2(c2) and 2(d2). The spin polarization along this orientation is not expected from the Rashba model because the effective magnetic field originates from the cross product $\vec{E} \times \vec{k}$, which is always orthogonal to $\vec{k}$. The Bi/InAs(110)-(2 × 1) surface does not contain any magnetic element, and hence, the observed complex spin polarization cannot be explained solely from the initial states. Thus, it is suggested that the photoexcitation process is playing some role in the observed complex spin texture.

B. Spin polarizations of the ground states obtained from theoretical calculations

To reveal the initial-state spin texture, we calculated the surface band structures by DFT, as shown in Fig. 3. The sizes

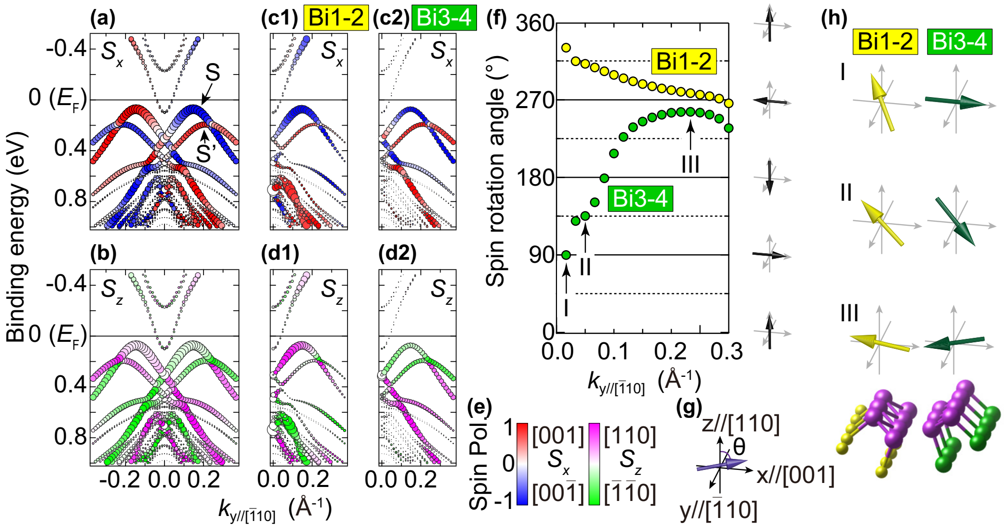

FIG. 3. Calculated spin-polarized band structure and spin texture in real space. (a)–(d2) Spin-polarized band dispersions obtained by DFT calculations. The radii of the circles are proportional to the sum of the contributions from all surface Bi atoms. Spin orientations are defined as (a), (c1), and (c2) in-plane (S_x) and (b), (d1), and (d2) out-of-plane (S_z) ones. (c1)–(d2) Surface bands with the spin orientations of each nonequivalent surface Bi chain. (e) Color scales represent spin polarizations: The blue-red (green-purple) color palette corresponds to the spins along the in-plane orientation S_x (out-of-plane orientation S_z). (f) Wave number dependence of the spin orientations in each Bi chain. (g) Definition of the spin rotation angle used in (f). (h) Typical cases of the spin orientations depending on $k_{y//[\bar{1}10]}$ in each Bi chain. Roman numbers correspond to the $k_{y//[\bar{1}10]}$ position shown by arrows in (f).

of the circles in Figs. 3(a) and 3(b) indicate the contribution of surface Bi atoms. Color scales [defined in Fig. 3(e)] show the degree of spin polarizations along S_x and S_z. The shapes of the surface bands (S and S') are qualitatively consistent with the results observed with ARPES and SARPES. All the spin-polarized structures are reversed from the sign of the wave number, indicating that the electronic structure obeys time-reversal symmetry. It should be noted that S_y spin polarization was not obtained in the DFT calculation, as expected from the time-reversal symmetry of the system confirmed above.

To obtain further insight into the surface spin texture, we decomposed the contributions to the surface bands from two inequivalent surface Bi chains: Bi1-2 and Bi3-4 [see Fig. 1(b) for the definition]. The radii of the circles in Figs. 3(c1)–3(d2) show that both Bi chains contribute to surface band S with nearly the same size. The in-plane spin polarizations S_x for chains Bi1-2 and Bi3-4 are shown in Figs. 3(c1) and 3(c2), respectively. Although they point [00$\bar{1}$] in most of the region of positive k_y, such spin polarization decreases near $\bar{\Gamma}$ and even changes the direction (pointing [001]) for Bi3-4. In a high-symmetry surface such as Pb/Ag(111) and Bi/Ag(111), similar spin inversion in a surface band could be attributed to wave function conversion of the $\mathbf{k}\cdot\mathbf{p}$ Hamiltonian [22]; ϕ_1 (ϕ_2) has $+S_x$ ($-S_x$), and a majority of the contributing wave function switches with the wave number, for example. However, in the current system, Bi/InAs(110)-(2 × 1), we found no such clear characteristics (Bi atoms 1 to 4 and each of the p_x, p_y, and p_z orbitals) to explain the spin inversion as well as the real-space spin texture between inequivalent Bi chains. On the contrary, the out-of-plane spin polarizations S_z of Bi chains are opposite each other, as shown in Figs. 3(d1) and 3(d2). This indicates that each Bi chain has independent spin polarization, even at the same (E, $\vec{k}$) points. In contrast to S_x, the S_z spin polarization is large around $\bar{\Gamma}$ and decreases in $k_y > 0.2$ Å^{-1}. This behavior of S_x and S_z indicates the rotation of the spin polarization of S depending on k_y.

To visualize the spin texture in real space, the spin rotation angle depending on the wave number was calculated for the S band. The results are shown in Fig. 3(f). The spin rotation angle is defined with $S_z = +1$ being the origin (0°) and $S_x = +1$ being 90°. Interestingly, the spin rotation angle of the S band varies continuously in the xz plane depending on the wave number, and the sign of the rotation is opposite between Bi1-2 and Bi3-4 in the region from the $\bar{\Gamma}$ point ($k_{y//[\bar{1}10]} = 0.0$ Å^{-1}) to near the top of the parabola ($k_{y//[\bar{1}10]} \sim 0.2$ Å^{-1}). This indicates that the sign reversal of the S_x polarization in Bi3-4 is the outcome of such a continuous spin rotation in the xz plane. Figure 3(h) depicts the spin orientation of each Bi chain in real space at some specific wave numbers indicated in Fig. 3(f). Near $\bar{\Gamma}$ (area I), the spin orientation in each chain is completely different. In area II, slightly closer to the apex of the parabolic band, the polarization direction is antiparallel, showing antiferromagnetic spin order. Near the apex of the parabola (area III), the spins of the two Bi chains become nearly parallel with a small S_z component. In this k_y region, the surface spin texture is similar to the spin structure expected for a normal Rashba-type spin texture, namely, the "ferromagnetic" case, compared to region II. Wave-number-dependent spin rotation in the Rashba system has already been reported [7], but such fertile spin orders, from the antiferromagnetic to nearly ferromagnetic cases between two inequivalent atomic chains, are not expected from ordinary Rashba systems.

C. Comparison between the observed photoelectron spectra and the calculated ground states

Here, we compare the calculated spin texture of the initial surface states with the experimentally observed spin-polarized

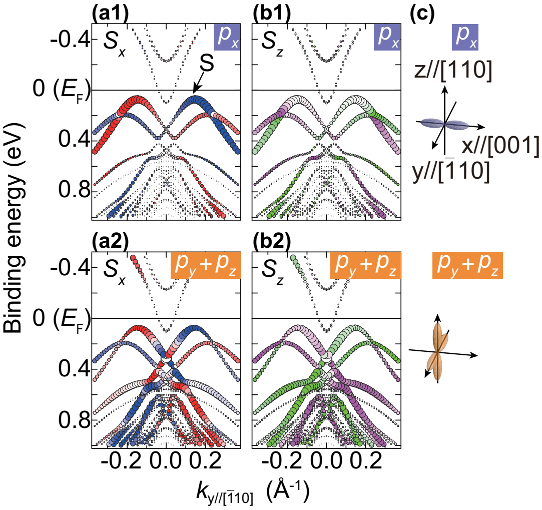

FIG. 4. Spin polarizations of photoelectrons decomposed based on the symmetries. (a1)–(b2) Calculated band dispersions shown in a manner similar to Fig. 3(a), but the radii of the circles are obtained by taking the Bi 6p (p_x, p_y, and p_z) atomic orbitals, which have (a1) and (b1) odd and (a2) and (b2) even symmetries with respect to the photon-incident plane in the SARPES experimental geometry. The colors of the circles are from the corresponding Bi 6p orbitals with S_x and S_z polarizations. (c) Schematics of the Bi 6p orbitals superposed on the coordinate axes.

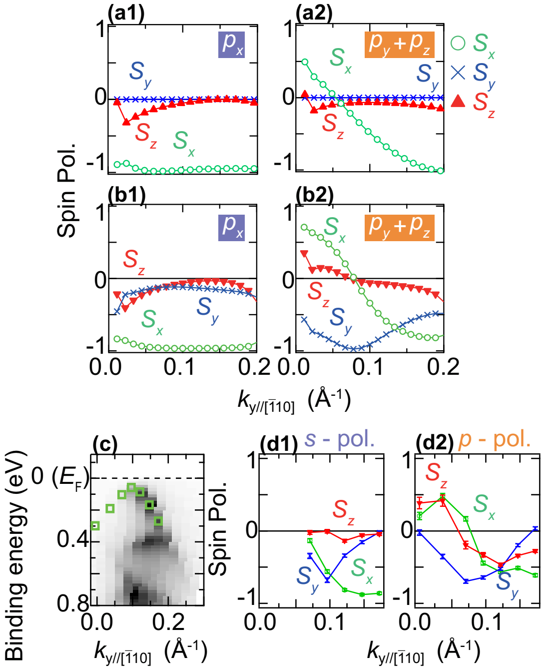

FIG. 5. Spin polarizations of the photoelectrons from the computational and experimental analysis. (a1) and (a2) Three-dimensional spin polarizations of the initial state obtained from the DFT calculation with (a1) p_x (odd) and (a2) $p_y + p_z$ (even) Bi orbitals of the S band. (b1) and (b2) Photoelectron spin polarizations with (b1) p_x and (b2) $p_y + p_z$ Bi orbitals calculated numerically by considering the photoelectron interference of two nonequivalent Bi chains. The phase difference of the wave function between the Bi1-2 and Bi3-4 chains was set to $2\pi/3$. See the Supplemental Material for details of the calculation [15]. (c) ARPES band mapping with the s-polarized photons. Square rectangles represent the regions where the spin polarizations in (d1) and (d2) are obtained. (d1) and (d2) Experimentally observed spin polarizations measured with (d1) s- and (d2) p-polarized photons.

photoelectron spectra. For this purpose, we decomposed the calculated Bi orbital wave functions to odd (p_x) and even (p_y and p_z) ones with respect to the measurement plane, as shown in Figs. 4(a1)–4(b2). The odd and even initial states should correspond to the photoelectrons excited by s- and p-polarized photons shown in Fig. 2, respectively, based on the selection rule of the electric dipole photoexcitation. The radii of the circles in Figs. 4(a1)–4(b2) are proportional to the surface Bi wave functions with odd or even parity. Odd (even) Bi wave functions shown in Figs. 4(a1) and 4(b1) [Figs. 4(a2) and 4(b2)] have a large contribution around (away from) $\bar{\Gamma}$ for surface band S. This trend is consistent with the small photoelectron intensity around $\bar{\Gamma}$ from s-polarized photons [Fig. 2(a)]. As for the spin polarization, the in-plane orientation (S_x) of S could reproduce the observed results. Although the spins of the odd wave functions [Fig. 4(a1)] are intense and monotonic, those of the even wave functions [Fig. 4(a2)] show the sign inversion from 0 Å^{-1} ($\bar{\Gamma}$) to 0.2 Å^{-1} (near the top of the parabolic band) in surface band S. In contrast to the in-plane case, the situation of the out-of-plane spins [S_z, shown in Figs. 4(d1) and 4(d2)] is complicated. Although nearly negligible values for the odd wave functions are consistent with the observed results [Figs. 2(c3)], the observed inversion [Figs. 2(d3)] is not reproduced for the even wave functions. Together with the exactly zero polarization parallel to k_y (S_y) in the calculation, it is obvious that the initial-state calculation is insufficient for understanding the observed spin polarization of photoelectrons.

The photoelectron interference effect in the spin-polarized states has already been discussed for topological materials Bi and Bi$_2$Se$_3$ [11–13,23]. If two or more wave functions with different spin polarizations are photoexcited simultaneously, the interference between them can result in a unique spin polarization of final-state photoelectrons. As shown in Fig. 3(f), Bi/InAs(110)-(2 × 1) has two inequivalent Bi chains with different spin orientations at each k_y. We adopted these two Bi chains as the different initial states and calculated their interference numerically during the spin-dependent photoexcitation process in a manner similar to that used in earlier works [13,23] (see Supplemental Material, Note 1, for details). Figures 5(a1) and 5(a2) are the spin polarizations of the initial states of the S bands obtained from our DFT calculation with the odd and even symmetries, respectively. Figure 5(b1) [Fig. 5(b2)] depicts simulated photoelectron spin polarizations corresponding to the initial states shown in Fig. 5(a1) [Fig. 5(a2)]. Figures 5(d1) and 5(d2) are the corresponding spin polarizations of the observed photoelectrons. For the odd states [Figs. 5(a1) and 5(d1)], monotonic polarizations with sizable S_x and small S_z in the calculation agree well with the experimental results. A decrease in S_x in the vicinity of $\bar{\Gamma}$ that appears in the experimental result does not appear in the calculation. The possible reason is that the experimental value is not so reliable owing to the vanishing photoelectron intensities. For the even states [Figs. 5(a2) and 5(d2)], the calculated directions of S_x and S_z are consistent with the corresponding experimental ones. The inversion of S_z is absent in the initial states [Fig. 5(a2)] but is propagated from S_x by the photoelectron interference. It should be noted that the spin polarization parallel to k (S_y) is also obtained in the calculation, in contrast to its absence in the initial states. Although this calculation is insufficient for reproducing some quantitative values, such as the spin polarization ratio S_x/S_z for the even states, it is sufficient for capturing the qualitative behavior of this complicated spin texture.

IV. CONCLUSION AND OUTLOOK

In this work, we have revealed the spin polarization of the surface states with quite a large degree of variety using a combination of spin- and angle-resolved photoelectron spectroscopy and theoretical calculation. The consistency of the numerical calculation and SARPES results supports the peculiar spin orders between neighboring Bi chains, fluctuating depending on the wave number, as shown in Fig. 3. It should be noted that a new mechanism is not required to explain such a spin texture in the surface ground states. As already observed in Weyl semimetals [24,25], spin polarization derived from SOI can point in arbitrary orientations as long as the surface symmetry operations permit it. The reason why the current result seems unnatural could be because most earlier works on the surface Rashba states were performed on simple surfaces. Therein, the number of inequivalent atoms was smaller, and the number of symmetry operations was larger than in the present Bi/InAs(110)-(2 × 1) case with only one mirror plane. The current results also exhibit that the excited electrons could have various, almost arbitrary spin polarizations depending on the photoexcitation conditions. Not only the fine tuning of the photon polarization [13] but also the wave number selection with the electronic states derived from many inequivalent wave functions can provide highly spin polarized electrons with the polarization orientations on demand.

The surface band S of Bi/InAs(110)-(2 × 1) appears to obey the surface Rashba effect, a paired parabolic dispersion with helical spin polarization [20]. However, the current result revealed that the actual spin and orbital constitution is considerably more complex than the simple Rashba model, as shown in Fig. 1. This indicates that such a model is too simple to represent a realistic system. Actually, other typical Rashba and topological systems, such as Bi_2Se_3 [12,23], Bi(111) [13], Pb/Ag(111), and Bi/Ag(111) [22,26], have multiple spin and orbital components. Because SOI itself is an interaction to mix the off-diagonal orbital characters with different spins [27,28], complex spin-orbital entanglement would be a general characteristic of the low-dimensional electronic states influenced by SOI. Some theoretical studies claim that such a mixture is essential for Rashba-type SOI [29,30].

ACKNOWLEDGMENTS

The SARPES measurements were jointly conducted with ISSP, The University of Tokyo. This work was also supported by JSPS KAKENHI (Grants Nos. JP20K03859, No. JP19H01830, No. JP18K03484, and No. JP20H04453).

[1] S. Kasahara, H. J. Shi, K. Hashimoto, S. Tonegawa, Y. Mizukami, T. Shibauchi, K. Sugimoto, T. Fukuda, T. Terashima, Andriy H. Nevidomskyy, and Y. Matsuda, Electronic nematicity above the structural and superconducting transition in $BaFe_2(As_{1-x}P_x)_2$, Nature (London) **486**, 382 (2012).

[2] I. Gierz, M. Lindroos, H. Höchst, C. R. Ast, and K. Kern, Graphene sublattice symmetry and isospin determined by circular dichroism in angle-resolved photoemission spectroscopy, Nano Lett. **12**, 3900 (2012).

[3] Y. A. Bychkov and E. I. Rashba, Oscillatory effects and the magnetic susceptibility of carriers in inversion layers, J. Phys. C **17**, 6039 (1984).

[4] M. Z. Hasan and C. L. Kane, Colloquium: Topological insulators, Rev. Mod. Phys. **82**, 3045 (2010).

[5] A. Manchon, H. C. Koo, J. Nitta, S. M. Frolov, and R. A. Duine, New perspectives for Rashba spin-orbit coupling, Nat. Mater. **14**, 871 (2015).

[6] W. Han, Y. Otani, and S. Maekawa, Quantum materials for spin and charge conversion, npj Quantum Mater. **3**, 27 (2018).

[7] K. Sakamoto, T. Oda, A. Kimura, K. Miyamoto, M. Tsujikawa, A. Imai, N. Ueno, H. Namatame, M. Taniguchi, P. E. J. Eriksson, and R. I. G. Uhrberg, Abrupt Rotation of the Rashba Spin to the Direction Perpendicular to the Surface, Phys. Rev. Lett. **102**, 096805 (2009).

[8] S. Souma, K. Kosaka, T. Sato, M. Komatsu, A. Takayama, T. Takahashi, M. Kriener, K. Segawa, and Y. Ando, Direct Measurement of the Out-of-Plane Spin Texture in the Dirac-Cone Surface State of a Topological Insulator, Phys. Rev. Lett. **106**, 216803 (2011).

[9] T. Okuda and A. Kimura, Spin- and angle-resolved photoemission of strongly spin-orbit coupled systems, J. Phys. Soc. Jpn. **82**, 021002 (2013).

[10] R. Suzuki, M. Sakano, Y. J. Zhang, R. Akashi, D. Morikawa, A. Harasawa, K. Yaji, K. Kuroda, K. Miyamoto, T. Okuda, K. Ishizaka, R. Arita, and Y. Iwasa, Valley-dependent spin polarization in bulk MoS_2 with broken inversion symmetry, Nat. Nanotechnol. **9**, 611 (2014).

[11] Z.-H. Zhu, C. N. Veenstra, S. Zhdanovich, M. P. Schneider, T. Okuda, K. Miyamoto, S.-Y. Zhu, H. Namatame, M. Taniguchi, M. W. Haverkort, I. S. Elfimov, and A. Damascelli, Photoelectron Spin-Polarization Control in the Topological Insulator Bi_2Se_3, Phys. Rev. Lett. **112**, 076802 (2014).

[12] K. Kuroda, K. Yaji, M. Nakayama, A. Harasawa, Y. Ishida, S. Watanabe, C.-T. Chen, T. Kondo, F. Komori, and S. Shin, Coherent control over three-dimensional spin polarization for the spin-orbit coupled surface state of Bi_2Se_3, Phys. Rev. B **94**, 165162 (2016).

[13] K. Yaji, K. Kuroda, S. Toyohisa, A. Harasawa, Y. Ishida, S. Watanabe, C. Chen, K. Kobayashi, F. Komori, and S. Shin, Spin-dependent quantum interference in photoemission process from spin-orbit coupled states, Nat. Commun. **8**, 14588 (2017).

[14] M. G. Betti, D. Berselli, C. Mariani, N. Jedrecy, M. Sauvage-Simkin, Y. Garreau, and R. Pinchaux, (1×2) Bi chain reconstruction on the InAs(110) surface, Phys. Rev. B **59**, 15760 (1999).

[15] See Supplemental Material at http://link.aps.org/supplemental/10.1103/PhysRevB.105.235141 for the additional experimental data set, LEED patterns and SARPES spectra, and a detailed calculation method to simulate the photoelectron spin polarization.

[16] K. Yaji, A. Harasawa, K. Kuroda, S. Toyohisa, M. Nakayama, Y. Ishida, A. Fukushima, S. Watanabe, C. Chen, F. Komori, and S. Shin, High-resolution three-dimensional spin- and angle-resolved photoelectron spectrometer using vacuum ultraviolet laser light, Rev. Sci. Instrum. **87**, 053111 (2016).

[17] P. Blaha, K. Schwarz, F. Tran, R. Laskowski, G. K. H. Madsen, and L. D. Marks, WIEN2k: An APW+lo program for calculating the properties of solids, J. Chem. Phys. **152**, 074101 (2020).

[18] A. D. Becke and E. R. Johnson, A simple effective potential for exchange, J. Chem. Phys. **124**, 221101 (2006).

[19] F. Tran and P. Blaha, Accurate Band Gaps of Semiconductors and Insulators with a Semilocal Exchange-Correlation Potential, Phys. Rev. Lett. **102**, 226401 (2009).

[20] T. Nakamura, Y. Ohtsubo, Y. Yamashita, S.-i. Ideta, K. Tanaka, K. Yaji, A. Harasawa, S. Shin, F. Komori, R. Yukawa, K. Horiba, H. Kumigashira, and S.-i. Kimura, Giant Rashba splitting of quasi-one-dimensional surface states on Bi/InAs(110)–(2×1), Phys. Rev. B **98**, 075431 (2018).

[21] S. Hüfner, *Photoelectron Spectroscopy* (Springer, Berlin, 2003).

[22] I. A. Nechaev and E. E. Krasovskii, Spin polarization by first-principles relativistic $\mathbf{k} \cdot \mathbf{p}$ theory: Application to the surface alloys $PbAg_2$ and $BiAg_2$, Phys. Rev. B **100**, 115432 (2019).

[23] Z.-H. Zhu, C. N. Veenstra, G. Levy, A. Ubaldini, P. Syers, N. P. Butch, J. Paglione, M. W. Haverkort, I. S. Elfimov, and A. Damascelli, Layer-by-Layer Entangled Spin-Orbital Texture of the Topological Surface State in Bi_2Se_3, Phys. Rev. Lett. **110**, 216401 (2013).

[24] S.-Y. Xu *et al.*, Spin Polarization and Texture of the Fermi Arcs in the Weyl Fermion Semimetal TaAs, Phys. Rev. Lett. **116**, 096801 (2016).

[25] B. Feng, Y.-H. Chan, Y. Feng, R.-Y. Liu, M.-Y. Chou, K. Kuroda, K. Yaji, A. Harasawa, P. Moras, A. Barinov, W. Malaeb, C. Bareille, T. Kondo, S. Shin, F. Komori, T.-C. Chiang, Y. Shi, and I. Matsuda, Spin texture in type-II Weyl semimetal WTe_2, Phys. Rev. B **94**, 195134 (2016).

[26] R. Noguchi, K. Kuroda, K. Yaji, K. Kobayashi, M. Sakano, A. Harasawa, T. Kondo, F. Komori, and S. Shin, Direct mapping of spin and orbital entangled wave functions under interband spin-orbit coupling of giant Rashba spin-split surface states, Phys. Rev. B **95**, 041111(R) (2017).

[27] D. J. Chadi, Spin-orbit splitting in crystalline and compositionally disordered semiconductors, Phys. Rev. B **16**, 790 (1977).

[28] L. Petersen and P. Hedegård, A simple tight-binding model of spin-orbit splitting of sp-derived surface states, Surf. Sci. **459**, 49 (2000).

[29] J. Premper, M. Trautmann, J. Henk, and P. Bruno, Spin-orbit splitting in an anisotropic two-dimensional electron gas, Phys. Rev. B **76**, 073310 (2007).

[30] H. Ishida, Rashba spin splitting of Shockley surface states on semi-infinite crystals, Phys. Rev. B **90**, 235422 (2014).